Structural, Microstructural, Magnetic, and Ferroelectric Properties of Ba^{2+}-Doped $BiFeO_3$ Nanocrystalline Multifferroic Material

Original Paper Published: 12 December 2017

Volume 31, pages 2501–2509, (2018) Cite this article

Journal of Superconductivity and Novel Magnetism

Aims and scope

Submit manuscript

Mahendra V. Shisode, Dhananjay N. Bhoyar, Pankaj P. Khirade & K. M. Jadhav

Abstract

Multiferroic barium-substituted nanocrystalline samples having the general formula $Bi_{1-x}Ba_xFeO_3$ (where x = 0.00, 0.05, 0.10, 0.15, 0.20, 0.25) were prepared by cost-effective sol–gel method using metal nitrates as oxidants. The prepared samples were annealed at 650 °C for 4

h using a muffle furnace. The influence of Ba^{2+} doping on the structural, microstructural, magnetic, and ferroelectric properties of bismuth ferrite (BFO) was studied systematically by standard techniques. All the samples were characterized by X-ray diffraction (XRD) technique, and the average crystallite size was calculated using Scherrer's formula. The surface morphology of the prepared nanocrystalline samples was studied using field emission scanning electron microscopy (FE-SEM) technique. FTIR spectra were obtained to confirm the formation of the perovskite structures. The elemental compositional details obtained were confirmed by energy dispersive spectrum (EDS) analysis. Room temperature magnetic measurements were carried out up to a field of 15 kOe, and the parent sample (BFO) shows weak ferromagnetism. Further on, Ba^{2+} substitution in BFO shows an increase in magnetization. *P*–*E* loops were obtained to study the ferroelectric properties of all the samples. Obtained enhancement in magnetic and ferroelectric properties at room temperature is of great interest within the research community due to its wide range of applications in memory storage, spintronics, sensors, and multi-functional devices.

1 Introduction

The materials with the simultaneous occurrence of at least two primary ferroic orders, i.e., anti/ferroelectricity and anti/ferromagnetism or ferroelasticity in a single phase, are called multiferroic or multifunctional materials (e.g., $BiFeO_3$). Bismuth ferrite has a rhombohedral distorted perovskite structure with space group R3c and having the general chemical formula ABO_3 where A and B are cations [1]. Since the last few decades, multiferroic materials have attracted many researchers due to their potential application in multifunctional devices like a giant electrical transformer to compact devices like sensors [2]. Despite the discovery of $BiFeO_3$ in 1960, bismuth ferrite powders are being preparedby various low-temperature wet-chemical methods such as mechano-chemical method, micro-emulsion method, a co-precipitation method, hydrothermal method, sonochemical method, sol-gel method, and some other routes [3,4,5,6,7,8,9]. To gain nanosize samples avoiding bismuth volatilization, low-temperature synthesis methods like sol-gel methods are developed. Among the various solution-based methods for synthesizing bismuth ferrite (BFO) nanoparticles, we chose the sol-gel method due to easy control of chemical composition and cost-effectiveness [10]. BFO is one of the most promising due to coupling between ferroelectric and magnetic ordering at room temperature, leading to room temperature device application. BFO exhibits higher ferroelectric Curie temperature ($T_C \sim 1103$ K) and a G-type antiferromagnetic ordering temperature ($T_N \sim 643$ K) [11, 12]. BFO material is important not only due to its high Neel and Curie temperatures but also due to its ferroelectric and ferromagnetic properties at room temperature. BFO is considered as the most likely candidate for magnetic storage or in the applications of spintronic devices [13]; a large leakage current due to oxygen vacancies or impurities are the major problem in $BiFeO_3$ [14]. The room temperature magnetoelectric coupling in pure-phase BFO makes it applicable for the fabrication of various emerging electronic devices like multiple state memories, magnetic data storage media, actuators, transducers, sensors, spintronics, and multifunctional devices [15]; also, the BFO nanoparticles are applicable in biomedical applications [16].

It is very difficult to prepare phase pure bismuth ferrite because of its narrow stability temperature range and because it produces secondary phases along with it. Doping with rare earth cations (La^{3+}, Pr^{3+}, Dy^{3+}, Sm^{3+}, etc.) and divalent cations (Mg^{2+}, Ca^{2+}, Ni^{2+}, Zn^{2+}, Sr^{2+}, Ba^{2+}, etc.) at the Bi site and doping by cations (Cr^{3+}, Mn^{3+}, Co^{3+}, Ti^{4+}, Nb^{5+}, etc.) at the Fe site

suppress the secondary phases and also alter the multiferroic properties of $BiFeO_3$ [17, 18]. Due to Ba^{2+} substitution in BFO at the Bi site, charge compensation is necessary which results in the formation of oxygen vacancies and also changes the cycloidal spin of BFO to a canted spin structure which results in net magnetization at room temperature [19]. The inspiration for the fabrication of Ba^{2+}-doped BFO comes from the interesting magnetic behavior shown by $BaFeO_3$. Charge compensation is necessary due to the substitution of Ba^{2+} in the Bi^{3+} site, which affects the centrosymmetry of FeO_6 octahedra and this may result in the formation of oxygen vacancies. Finally, this leads to the alteration of the multiferroic properties of BFO.

In the present work, multiferroic nanocrystalline samples with the general formula $Bi_{1-x}Ba_xFeO_3$ (where $x = 0.0, 0.05, 0.10, 0.15, 0.20, 0.25$) were synthesized by a sol-gel method using metal nitrates as a starting material. A study was conducted on the effect of Ba doping in BFO on the structural, magnetic, and ferroelectric properties of bismuth ferrite samples.

2 Experimental

2.1 Materials

Analytical-grade bismuth nitrate pentahydrate ($Bi(NO_3)_3 \cdot 5H_2O$), ferric nitrate nonahydrate ($Fe(NO_3)_3 \cdot 9H_2O$, 99%, *Merck*), barium nitrate ($Ba(NO_3)_2$, 99%, *Merck*), and ethylene glycol (EG, $C_2H_6O_2$, 99%, *Merck*) were used in appropriate amounts without any further purification.

2.2 Synthesis

$Bi_{1-x}Ba_xFeO_3$ (where $x = 0.00, 0.05, 0.10, 0.15, 0.20, 0.25$) nanoparticles were successfully synthesized by sol-gel method at room temperature. High-purity bismuth nitrate ($Bi(NO_3)_3 \cdot 5H_2O$), ferric nitrate ($Fe(NO_3)_3 \cdot 9H_2O$), and barium nitrate ($Ba(NO_3)_2$) were used as sources of Bi^{3+}, Fe^{3+}, and Ba^{2+} for the synthesis of nanocrystalline samples. Stoichiometric amounts of bismuth nitrate ($Bi(NO_3)_3 \cdot 5H_2O$), ferric nitrate ($Fe(NO_3)_3 \cdot 9H_2O$), and barium nitrate ($Ba(NO_3)_3$) were separately dissolved in the ethylene glycol with a stirring speed of around 350–450 rpm. Then, these solutions were mixed in a 1000-ml beaker. The mixed solution was stirred at 50 °C for 3 h to obtain a homogeneous solution. The xerogel was obtained by evaporating the precursor solution on a hot plate at 70 °C for about 5 h; the viscous gel starts to

bubble giving a large amount of gases. Then, it was ground into powder using a mortar and pestle and heated at 120 °C for 1 h, followed by treatment at 300 °C for 2 h to remove ethylene glycol (EG). The cooled powder was finely ground and sintered at 650 °C for 4 h and then cooled at room temperature. Lastly, the quenched powder was first washed with diluted nitric acid (10% in volume fraction) to dissolve a small amount of bismuth salt or oxide produced by the excess of Bi and then the powder was washed with deionized water with the help of a funnel and filter paper (Whatman no. 42). Using a hydraulic press, each sample was compressed and the pellets 1 cm in diameter were prepared and sintered at 800 °C for 1 h in a muffle furnace in the air atmosphere to study the ferroelectric properties. The nanocrystalline samples with different concentrations were characterized using standard measurement techniques, and the results are described as follows.

2.3 Characterizations

All the sintered samples were characterized by X-ray diffraction (XRD) technique to study the structure and phase purity using a model (X-Ray Diffraction System Ultima IV of Rigaku Corporation, Japan) at room temperature. The XRD patterns were recorded using Cu-Kα radiation (λ = 1.540598 Å) operated at 45 kV with 40 mA. Fourier transform infrared spectroscopies (FTIR) of the prepared samples were studied in the wave number range 4000–400 cm^{-1} (PerkinElmer spectrum). The surface morphology and microstructure of the prepared samples were analyzed using field emission scanning electron microscopy (FE-SEM, Hitachi Model-S-4800). The magnetic properties of the samples were measured using a VSM (Lake Shore Cryotronics) at a maximum field of 15 kOe at room temperature. Ferroelectric hysteresis loops were studied by a P-E loop tracer (Marine India Pvt. Ltd.).

3 Results and Discussion

3.1 Structural Analysis

Figure 1 shows X-ray diffraction (XRD) patterns of $Bi_{1-x}Ba_xFeO_3$ (where x = 0.00, 0.05, 0.10, 0.15, 0.20, 0.25)nanoparticles at room temperature. Figure 1 shows strong reflection peaks and the diffraction peaks of $Bi_{1-x}Ba_xFeO_3$ samples were indexed to a rhombohedral-hexagonal structure (R3c space group) which is in agreement with earlier results [20]. The broad and intense nature of the XRD pattern as obtained confirms that samples are in nanosize form. A

few secondary phases as $Bi_2Fe_4O_3$ and $Bi_{25}FeO_{39}$ were observed in the undoped sample and which disappeared in Ba^{2+}-doped BFO samples. It is observed from the XRD patterns that the impurity phases were reduced significantly for Ba-substituted BFO. All the peaks were indexed with their respective Miller indices as shown in Fig. 1 according to the hexagonal system of basis, and it is in agreement with perovskite bismuth ferrite (JCPDS card no-1518). XRD data were used to find structural parameters as the lattice constant (a = b and c), average crystallite size (D), X-ray density (d_X), bulk density (ρ_B), volume (V), and average grain size (G) as tabulated in Table 1. The average crystallite size was calculated by using Debye-Scherrer's formula [21].

$$ D=\frac{0.9\lambda} {\beta \text{cos}\theta} $$

(1)

The average crystallite size of the diffraction pattern was found in the range 44 to 29 nm. The average crystallite size of the diffraction patterns was found to be less than the period of spiral modulated spin order that is 62 nm. The analysis of the XRD pattern confirms lattice parameters (a and c) based on hexagonal distortion of the rhombohedral unit cell with space group R3c as shown in Table 1 using (2).

$$ \frac{1}{d}=\frac{4}{3}\frac{(h^{2 } +hk+k^{2})}{a^{2}}+ \frac{l^{2}}{c^{2}} $$

(2)

where d is the inter-planar spacing distance of the unit cell, a and c are lattice parameters, and (hkl) are Miller indices. Figure 2 shows the graph of the lattice parameter versus Ba content x which reveals that the lattice parameter increases with the Ba concentration increases. The increase in lattice parameter can be attributed to the large difference in ionic radii of doped Ba^{2+} (1.35 Å) and Bi^{3+} (1.03 Å) ions. The bulk density ρ_B of the pellets was measured using the Archimedes principle using water as a solvent having a density of ρ = 0.997 g/cm^3 using the following equation [22]:

$$ \rho _{\mathrm{B}}=\frac{w_{\text{dry}}}{w_{\text{wet}}-w_{\text{sus}}}\times

d_{\mathrm{H}_{2}\mathrm{O}} $$

(3)

where w_{wet} and w_{dry} are the wet and dry weights of the pellets subsequently measured in the air before and after drying at 100 °C for 24 h and w_{sus} is the suspended weight in water of each pellet. The computed values of the lattice parameter as listed in Table 1 increase with increasing Ba concentration obeying the well-known Vegard's law [23]. The diffraction patterns of pure and Ba-doped samples having the R3c space group are shown in Fig. 1.

Fig. 1

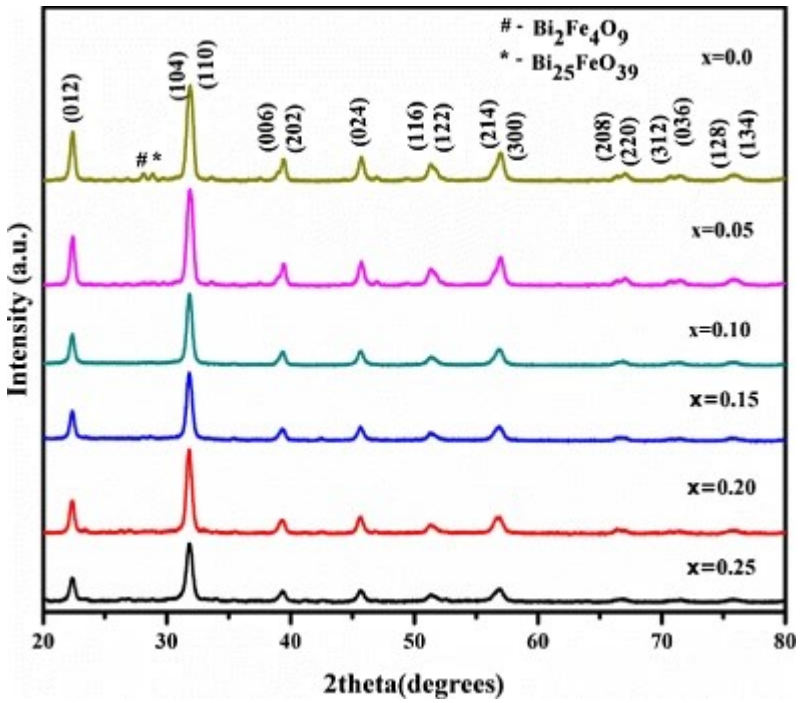

XRD patterns of the nanocrystalline samples of $Bi_{1-x}Ba_xFeO_3$ (where x = 0.0, 0.05, 0.10, 0.15, 0.20, 0.25)

Table 1 Lattice constant ($a = b, c$), X-ray density (d_X), bulk density (ρ_B), volume (V), crystallite size (D), and grain size (G)

Fig. 2

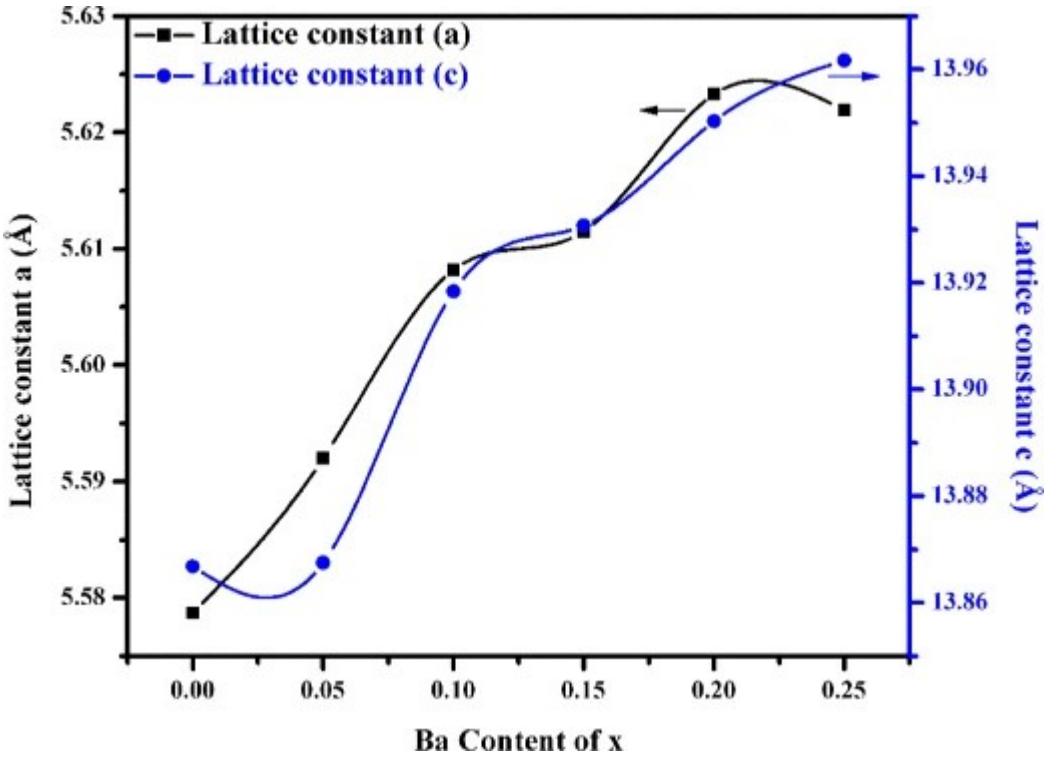

Lattice constants *a* and *c* as a function Ba content *x* for $Bi_{1-x}Ba_xFeO_3$

3.2 Surface Morphology

Figure 3a, b shows the microstructure and surface morphology of undoped and doped $BiFeO_3$ samples observed using FE-SEM. The obtained photographs reveal uniformly distributed densely packed grains having well-defined boundaries. The photos show the morphology of all the nanoparticles to be almost spherical and with an average grain size of 68–98 nm which is in agreement with the obtained values from Debye-Scherrer's formula. Ba^{2+} ions doping in BFO show a significant decrease in grain size [24]. This may be attributed to the difference in the ionic radius of Bi^{+3} (1.03 Å) and Ba^{2+} (1.35 Å).

Fig. 3

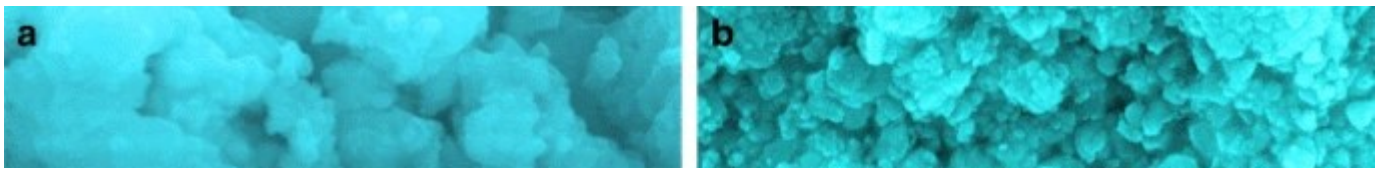

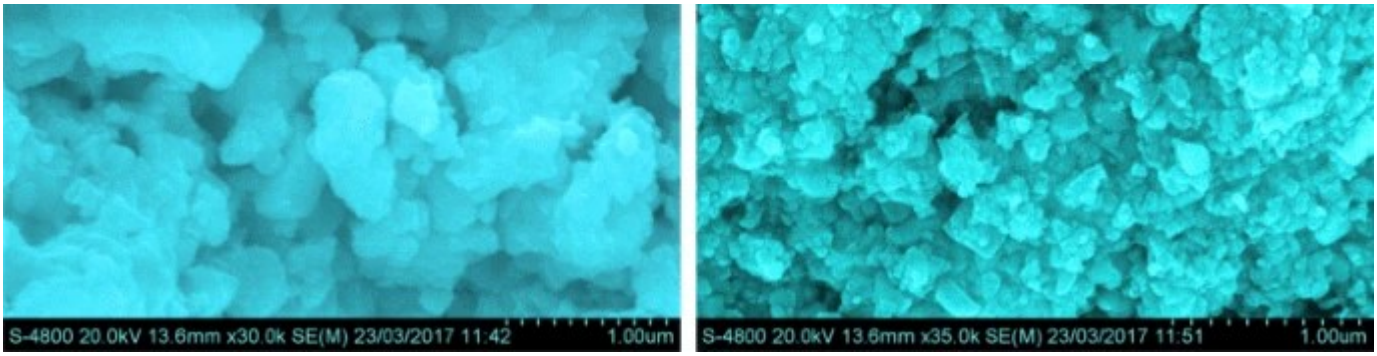

a, b Typical images of FE-SEM for $Bi_{1-x}Ba_xFeO_3$ (where x = 0.0, 0.10) nanocrystalline samples

3.3 FTIR Analysis

Figure 4 shows FTIR spectra of $Bi_{1-x}Ba_xFeO_3$ (where x = 0.00, 0.05, 0.10, 0.15, 0.20, 0.25) nanocrystalline samples, calcined at 650 °C to confirm the Ba^{2+} doping in $BiFeO_3$. Different wide-range bands are observed for all the samples at a wave number range of 4000–400 cm^{-1} which are the characteristics of different functional groups. The metal oxygen band in the region 600–400 cm^{-1} can confirm the formation of perovskite structure in all the samples [25]. The absorption band around 443 and 552 cm^{-1} is attributed to stretching vibration of the Fe–O bond in the FeO_6 octahedral unit and also due to the BiO_6 octahedral structural unit. From the FTIR plot, it is observed that Ba^{2+} substitution in BFO changes the nature of the absorption peak which is expected as the Fe–O bond length and bond angle change in doped samples. The BFO nanocrystalline compound shows Fe–O absorption at 811 cm^{-1} because of its crystalline phase. The signature of presence of trapped nitrates is seen around 1384 cm^{-1}. The absorption band around 1634 cm^{-1} is attributed to H–O–H bending vibration [26]. The presence of a peak around 2300 cm^{-1} can be attributed to the nitrile formation [27], while the broad band around 3600–3000 cm^{-1} is assigned to the antisymmetric and symmetric stretching of the OH group. Due to CO_2 elimination, porous samples can be created; for high-temperature applicability, there is a need of carbonate-free samples which is obtained.

Fig. 4

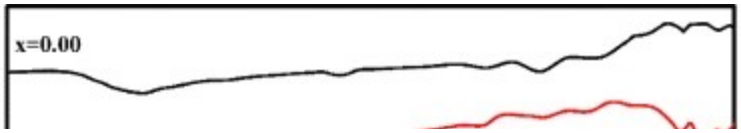

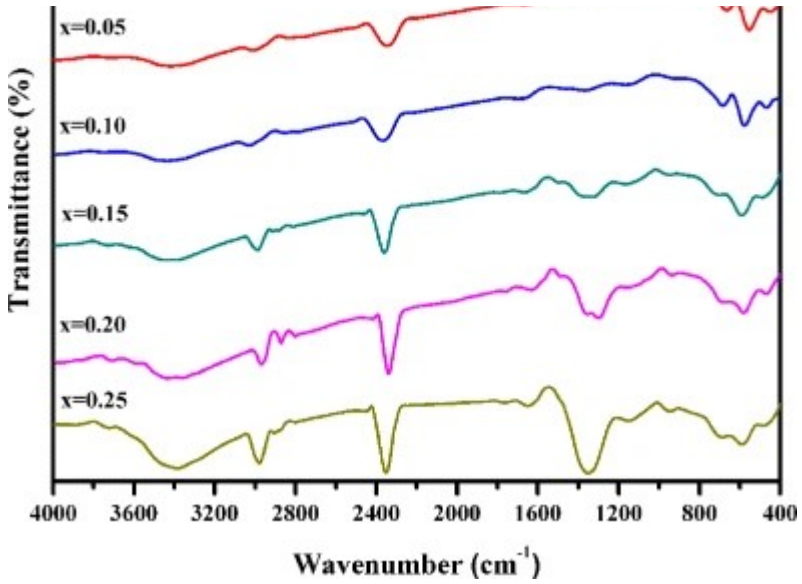

FTIR spectra of $Bi_{1-x}Ba_xFeO_3$ (where x = 0.0, 0.05, 0.10, 0.15, 0.20, 0.25) nanocrystalline samples

Figure 5 shows the typical image of the EDS pattern of a $Bi_{1-x}Ba_xFeO_3$ (where x = 0.0) nanocrystalline sample confirmed the presence of elements in the appropriate proportion with maintained stoichiometry in the prepared sample with an error of around 3%. EDS confirmed that the raw materials used for the synthesis have performed a complete chemical reaction to form the required perovskite structured $Bi_{1-x}Ba_xFeO_3$ nanocrystalline samples.

Fig. 5

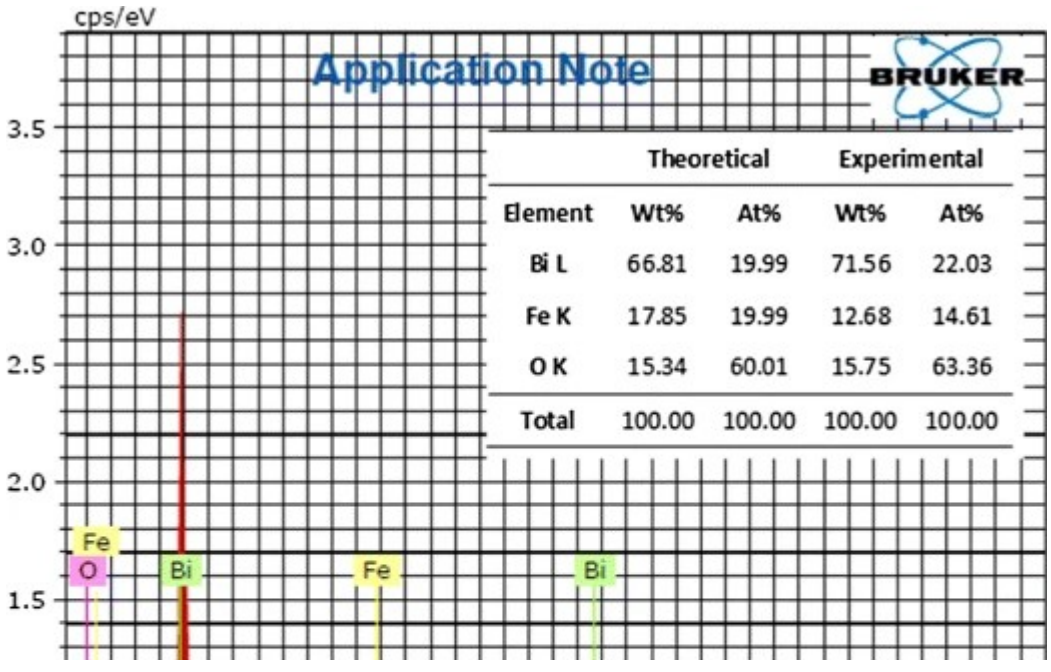

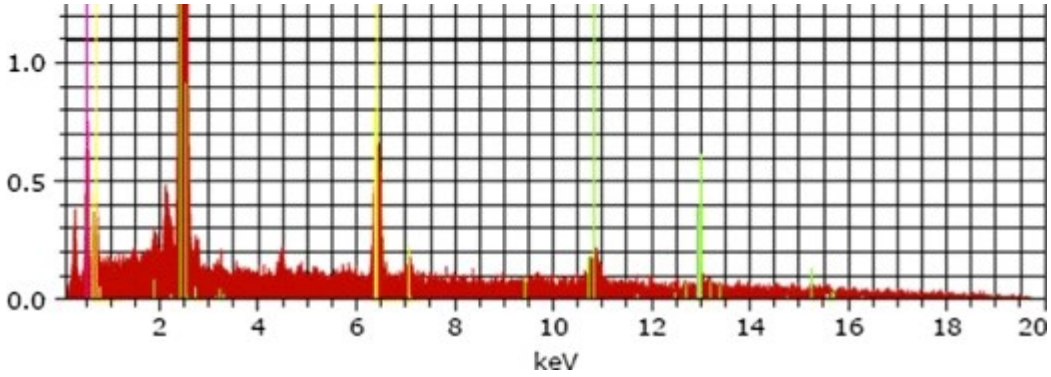

Typical image of EDAX for $Bi_{1-x}Ba_xFeO_3$ (where $x = 0.00$) nanocrystalline samples

3.4 Magnetic Properties

Figure 6 shows the $M-H$ hysteresis loops of the prepared samples of $Bi_{1-x}Ba_xFeO_3$ (where x = 0.00, 0.10, 0.15, 0.20, 0.25) recorded at room temperature using a vibrating sample magnetometer (VSM). The values of different magnetic parameters such as saturation magnetization (M_s), remanence magnetization (M_r), and coercivity (H_c) were obtained by $M-H$ plots. The hysteresis loop of the pure sample ($x = 0.0$) is almost a straight line passing through the origin exhibiting magnetization of 0.983 emu/g at the highest field of 15 kOe. Figure 7 shows saturation magnetization (M_s) and coercivity (H_c) as a function of Ba content x for $BiFeO_3$. From Table 2, it is observed that the values of saturation magnetization increase as Ba^{2+} doping concentration increases from 0.0983 to 3.006 emu/g. The reason for the origin of magnetization and increase in magnetization may be the variation of valence states of Fe in BFO and doping Ba at the Bi site will require Fe^{3+} charge compensation which results in the formation of Fe^{4+} or oxygen vacancies; the former may distribute statistically with Fe^{3+} in the octahedron in $Bi_{1-x}Ba_xFeO_3$. This leads to a net magnetization and ferromagnetism [28]. A further change in size and surface morphology of samples may also contribute to the increase in the magnetic moment by destroying the cycloid magnetic structure.

Fig. 6

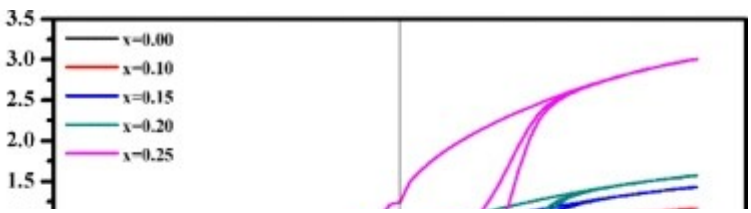

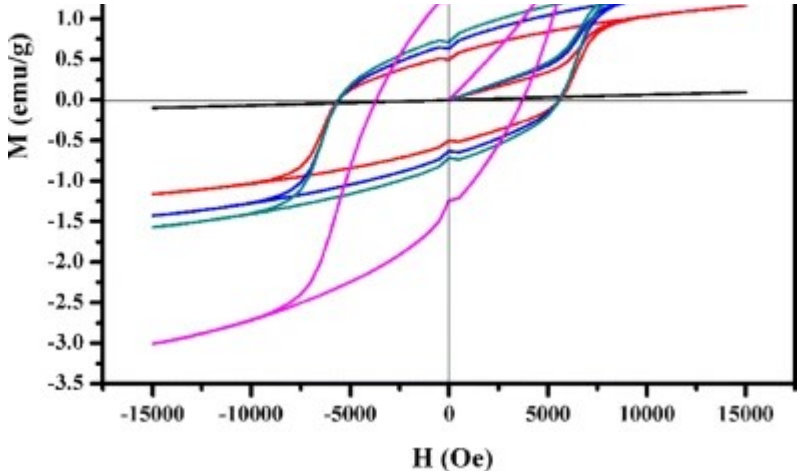

Room temperature magnetic hysteresis loops obtained for $Bi_{1-x}Ba_xFeO_3$ (where x = 0.00, 0.10, 0.15, 0.20, 0.25) nanocrystalline samples by VSM

Fig. 7

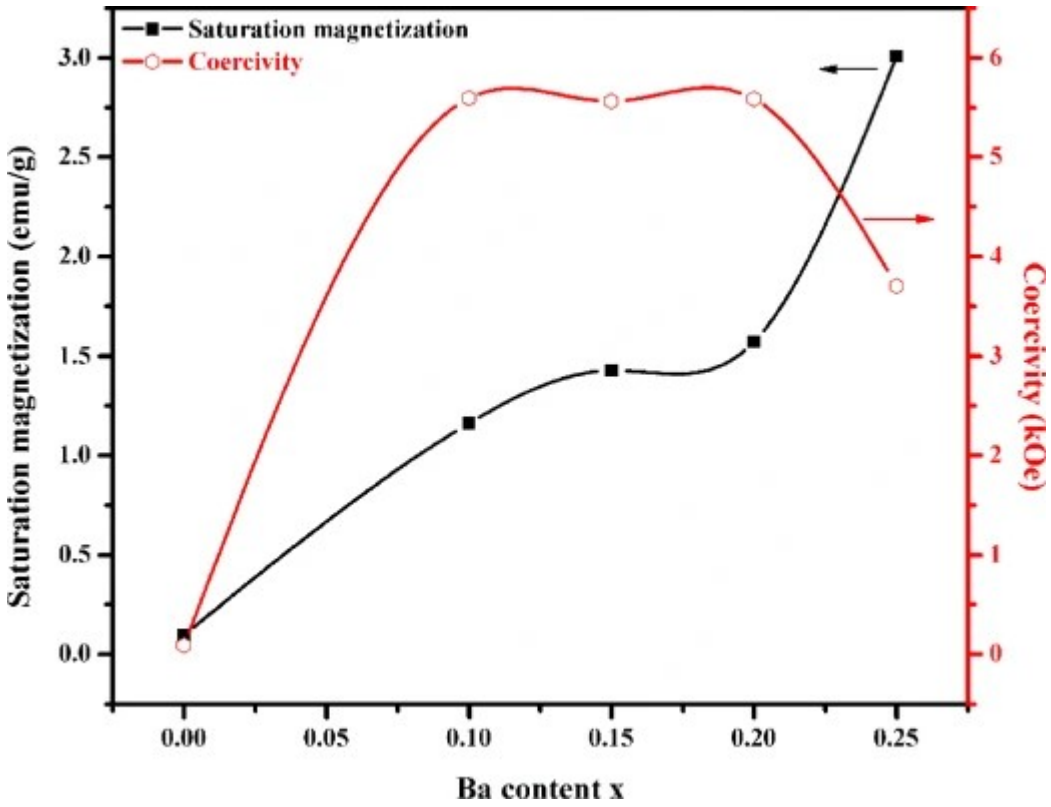

Saturation magnetization M_S and coercivity (H_C) as a function of Ba content x for $BiFeO_3$

Table 2 Saturation magnetization (M_s), remanence magnetization (M_r), coercivity (H_c), remanence ratio (M_r/M_s), magneton number (n_B)

The values of saturation magnetization and coercivity can be used to calculate the important magnetic parameter like magneton number (n_B). The magneton number for the entire Ba-substituted BFO samples can be calculated by using the relation [29]

$$ n_{\mathrm{B}}=\frac{M\cdot M_{\mathrm{s}}}{N_{\mathrm{A}}\cdot \mu _{\mathrm{B}}} $$

(4)

where M is the molecular weight of the different compositions of bismuth ferrite and M_s is the saturation magnetization (emu/g) at a particular composition. $N_A \mu_B$ is the constant equal to 5585. The obtained values of the magneton number increase as the Ba content increases in BFO as shown in Table 2. This increase in the magneton number is attributed to the increase in the exchange interactions between Bi and Ba cations which finally in- crease the net magnetization [30].

3.5 Ferroelectric Properties

Figure 8 shows the P–E loops of the nanocrystalline $Bi_{1-x}Ba_xFeO_3$ (where x = 0.00, 0.05, 0.10, 0.15, 0.20, 0.25) samples at room temperature measured at a frequency of 50 Hz. The loops of all the samples show unsaturated hysteresis loops with a roundish shape, which is due to a large leakage current [31]. It is very difficult to get good ferroelectric properties in perovskite bismuth ferrite due to the presence of oxygen vacancies [32]. With Ba substitution in BFO, better ferroelectric properties can be observed. The figure indicates that maximum P_r = 5.44 μC/cm^2 was found for x = 0.05 mol% with P_{max} = 5.51 μC/cm^2. All prepared samples exhibit an unsaturated hysteresis loop at the maximum electric field of 5 kV/cm. The observed roundish hysteresis loops are due to a large leakage current which can overshadow the real contribution from the reorientation of electrical dipoles. From Fig. 8, it can be seen that the leakage current is less or negligible in Ba-doped samples than in the undoped sample.

Fig. 8

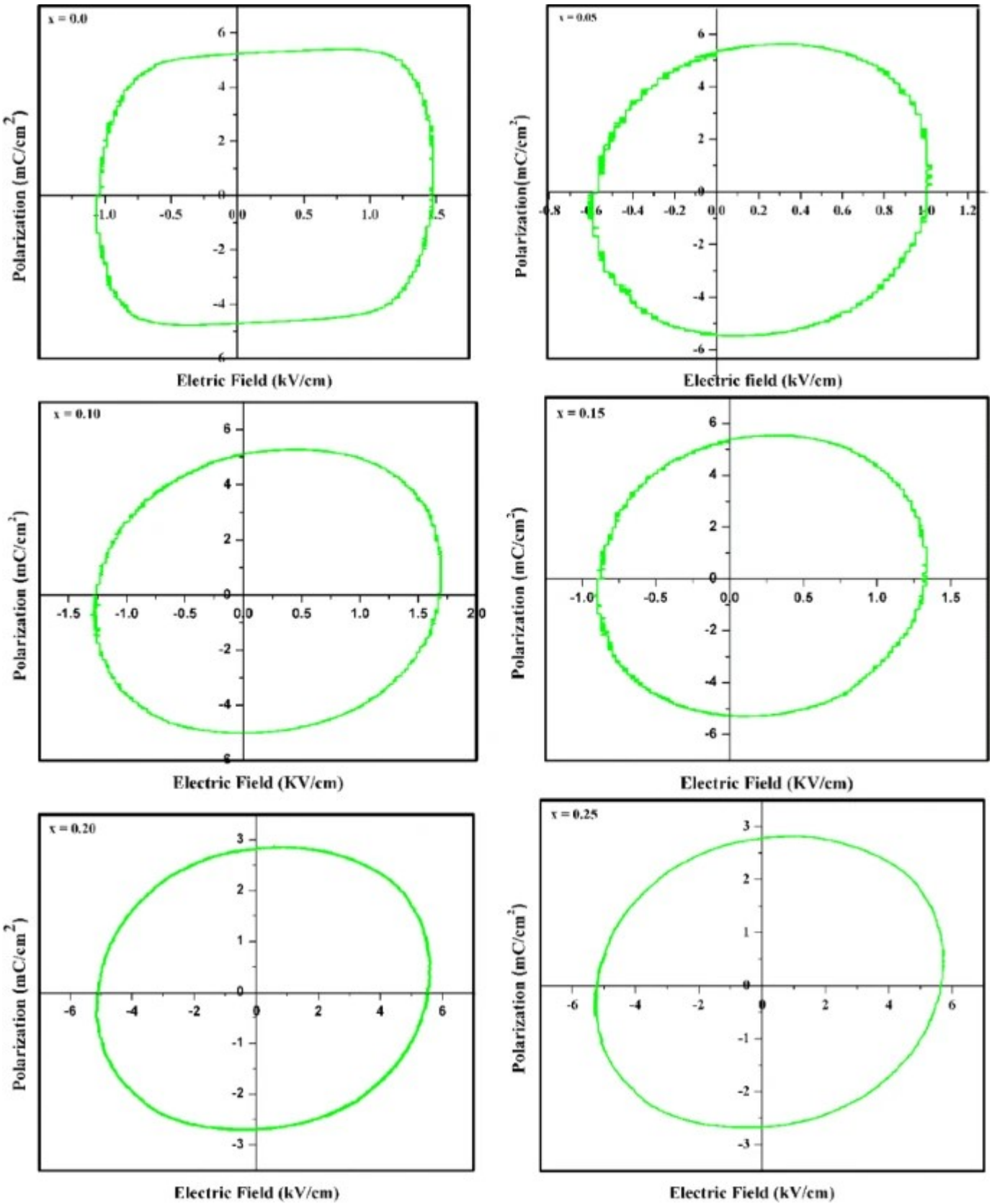

P–*E* loops of $Bi_{1-x}Ba_xFeO_3$ (where $x = 0.0, 0.05, 0.10, 0.15, 0.20, 0.25$) nanocrystalline samples measured at 5 kV/cm fields

4 Conclusion

The nanocrystalline $Bi_{1-x}Ba_xFeO_3$ (where x = 0.00, 0.05, 0.10, 0.15, 0.20, 0.25) system was successfully prepared by sol–gel route sintered at 650 °C. Effects of Ba^{2+} substitution on the structural, morphological, magnetic, and ferroelectric properties have been studied. The XRD study revealed that the structural transition from rhombohedral to hexagonal happens on increasing Ba^{2+} concentration in BFO which is in agreement with earlier reported data. These enhanced magnetic and ferroelectric properties of BFO nanoparticles can be potentially useful in data storage, actuators, sensors, transducers, and spintronic device applications. The lattice parameter (a and c) increases linearly with Ba^{2+} doping, obeying Vegard's law. The surface morphology of the samples determined using FE-SEM exhibited that the grain size was decreased as the Ba^{2+} concentration was increased in BFO. The EDS analysis confirms the prepared samples were near stoichiometry. Enhanced magnetic and ferroelectric properties were obtained on increasing Ba^{2+} concentration in BFO. These results suggest that the barium-doped bismuth ferrite nanoparticles are a good candidate for data storage applications and in multifunctional devices. Lastly, the simultaneous existence of ferromagnetic and ferroelectric hysteresis loops in Ba-substituted $BiFeO_3$ multiferroic materials at room temperature makes it a potential candidate for information storage, spintronics, and sensor devices.

References

1. Chhabra, K., Sharma, P.G.: Preparation and characterization of (1-x) BiFeO3-xNiFe2O4 (x = 0 0.3) composite (2012)

2. Tsymbal, E., Gruverman, A., Garcia, V., Bibes, M., Barthélémy, A.: Ferroelectric and multiferroic tunnel junctions. MRS Bullet. 37(02), 138–143 (2012)

Article Google Scholar

3. Fischer, P., Polomska, M., Sosnowska, I., Szymanski, M.: Temperature dependence of the crystal and magnetic structures of BiFeO3. J. Phys. C: Solid State Phys. 13(10), 1931 (1980)

Article ADS Google Scholar

4. Sharif, M.K., Khan, M.A., Hussain, A., Iqbal, F., Shakir, I., Murtaza, G., Akhtar, M.N., Ahmad, M., Warsi, M.F.: Synthesis and characterization of Zr and Mg doped BiFeO 3 nanocrystalline multiferroics via micro emulsion route. J. Alloys Compd. 667, 329–340 (2016)

Article Google Scholar

5. Xu, J.-H., Ke, H., Jia, D.-C., Wang, W., Zhou, Y.: Low-temperature synthesis of BiFeO 3 nanopowders via a sol–gel method. J. Alloys Compd. 472(1), 473–477 (2009)

Article Google Scholar

6. Das, N., Majumdar, R., Sen, A., Maiti, H.S.: Nanosized bismuth ferrite powder prepared through sonochemical and microemulsion techniques. Mater. Lett. 61(10), 2100–2104 (2007)

Article Google Scholar

7. Comyn, T.P., Kanguwe, D.F., He, J., Brown, A.P.: Synthesis of bismuth ferrite lead titanate nano-powders and ceramics using chemical co-precipitation. J. Eur. Ceram. Soc. 28(11), 2233–2238 (2008)

Article Google Scholar

8. Chen, X.-Z., Qiu, Z.-C., Zhou, J.-P., Zhu, G., Bian, X.-B., Liu, P.: Large-scale growth and shape evolution of bismuth ferrite particles with a hydrothermal method. Mater. Chem. Phys. 126(3), 560–567 (2011)

Article Google Scholar

9. Zhou, M., Li, W., Du, Y., Kong, D., Wang, Z., Meng, Y., Sun, X., Yan, T., Kong, D., You, J.: Hydrothermal synthesis of bismuth ferrite Fenton-like catalysts and their properties. J. Nanoparticle Res. 18(11), 346 (2016). https://doi.org/10.1007/s11051-016-3665-x

Article ADS Google Scholar

10. Khirade, P.P., Birajdar, S.D., Raut, A., Jadhav, K.: Multiferroic iron doped BaTiO 3 nanoceramics synthesized by sol-gel auto combustion: influence of iron on physical properties. Ceram. Int. 42(10), 12441–12451 (2016)

Article Google Scholar

11. Gautam, A., Rangra, V., Uniyal, P., Yadav, K.: Influence of Ti on multiferroic properties of Bi 0.8 Ba 0.2 Fe 1- x Ti x O 3 ceramics. In: 2011 International Symposium on Applications of Ferroelectrics (ISAF/PFM) and 2011 International Symposium on Piezoresponse Force Microscopy and Nanoscale Phenomena in Polar Materials, pp 1–4. IEEE (2011)

12. Manzoor, A., Hasanain, S.K., Mumtaz, A., Bertino, M.F., Franzel, L.: Effects of size and oxygen annealing on the multiferroic behavior of bismuth ferrite nanoparticles. J. Nanoparticle Res. 14(12), 1310 (2012). https://doi.org/10.1007/s11051-012-1310-x

Article ADS Google Scholar

13. Burr, G.W., Kurdi, B.N., Scott, J.C., Lam, C.H., Gopalakrishnan, K., Shenoy, R.S.: Overview of candidate device technologies for storage-class memory. IBM J. Res. Dev. 52(4.5), 449–464 (2008)

Article Google Scholar

14. Das, R., Mandal, K.: Magnetic, ferroelectric and magnetoelectric properties of Ba-doped BiFeO 3. J. Magn. Magn. Mater. 324(11), 1913–1918 (2012)

Article ADS Google Scholar

15. Gupta, R., Shah, J., Chaudhary, S., Singh, S., Kotnala, R.K.: Magnetoelectric coupling-induced anisotropy in multiferroic nanocomposite (1 - x)BiFeO3–xBaTiO3. J. Nanoparticle Res. 15(10), 2004 (2013). https://doi.org/10.1007/s11051-013-2004-8

Article ADS Google Scholar

16. Passemard, S., Staedler, D., Sonego, G., Magouroux, T., Schneiter, G.S., Juillerat-Jeanneret, L., Bonacina, L., Gerber-Lemaire, S.: Functionalized bismuth ferrite harmonic nanoparticles for cancer cells labeling and imaging. J. Nanoparticle Res. 17(10), 414 (2015). https://doi.org/10.1007/s11051-015-3218-8

Article ADS Google Scholar

17. Yao, Y., Liu, W., Chan, Y., Leung, C., Mak, C., Ploss, B.: Studies of rare-earth-doped BiFeO3 ceramics. Int. J. Appl. Ceram. Technol. 8(5), 1246–1253 (2011)

Article Google Scholar

18. Bhushan, B., Basumallick, A., Bandopadhyay, S., Vasanthacharya, N., Das, D.: Effect of alkaline earth metal doping on thermal, optical, magnetic and dielectric properties of BiFeO3 nanoparticles. J. Phys. D: Appl. Phys. 42(6), 065004 (2009)

Article ADS Google Scholar

19. Wang, D., Goh, W., Ning, M., Ong, C.: Effect of Ba doping on magnetic, ferroelectric, and magnetoelectric properties in mutiferroic Bi Fe O 3 at room temperature. Appl. Phys. Lett. 88(21), 212907 (2006)

Article ADS Google Scholar

20. El–Desoky, M., Ayoua, M., Mostafa, M., Ahmed, M.: Multiferroic properties of nanostructured barium doped bismuth ferrite. J. Magn. Magn. Mater. 404, 68–73 (2016)

Article ADS Google Scholar

21. Kharat, P.B., Shisode, M., Birajdar, S., Bhoyar, D., Jadhav, K.: Synthesis and characterization of water based NiFe2O4 ferrofluid, vol. 1, p. 050122. AIP Publishing (2017)

22. Khirade, P.P., Birajdar, S.D., Raut, A., Jadhav, K.: Effect of Fe–substitution on phase transformation, optical, electrical and dielectrical properties of BaTiO3 nanoceramics synthesized by sol-gel auto combustion method. J. Electroceram. 37(1-4), 110–120 (2016)

Article Google Scholar

23. Humbe, A.V., Nawle, A.C., Shinde, A., Jadhav, K.: Impact of Jahn Teller ion on magnetic and semiconducting behaviour of Ni-Zn spinel ferrite synthesized by nitrate-citrate route. J. Alloys Compd. 691, 343–354 (2017)

Article Google Scholar

24. Li, M., Ning, M., Ma, Y., Wu, Q., Ong, C.: Room temperature ferroelectric, ferromagnetic and magnetoelectric properties of Ba-doped BiFeO3 thin films. J. Phys. D: Appl. Phys. 40(6), 1603 (2007)

Article ADS Google Scholar

25. Raghavender, A., Hong, N.H.: Effects of Mn doping on structural and magnetic properties

of multiferroic BiFeO 3 nanograins made by sol-gel method. J. Magn. 16(1), 19–22 (2011)

Article Google Scholar

26. Vijayasundaram, S., Suresh, G., Kanagadurai, R.: Synthesis, thermal, structural, and magnetic properties of phase-pure nanocrystalline BiFeO3 via wet chemical route. Appl. Phys. A 121(2), 681–688 (2015)

Article ADS Google Scholar

27. Sankar Ganesh, R., Sharma, S.K., Sankar, S., Divyapriya, B., Durgadevi, E., Raji, P., Ponnusamy, S., Muthamizhchelvan, C., Hayakawa, Y., Kim, D.Y.: Microstructure, structural, optical and piezoelectric properties of BiFeO3 nanopowder synthesized from sol-gel. Curr. Appl. Phys. 17(3), 409–416 (2017). https://doi.org/10.1016/j.cap.2016.12.008

Article ADS Google Scholar

28. Chaudhuri, A., Mandal, K.: Study of structural, ferromagnetic and ferroelectric properties of nanostructured barium doped bismuth ferrite. J. Magn. Magn. Mater. 353, 57–64 (2014)

Article ADS Google Scholar

29. Patange, S., Shirsath, S.E., Toksha, B., Jadhav, S.S., Jadhav, K.: Electrical and magnetic properties of Cr 3+ substituted nano- crystalline nickel ferrite. J. Appl. Phys. 106(2), 023914 (2009)

Article ADS Google Scholar

30. Khan, U., Adeela, N., Javed, K., Riaz, S., Ali, H., Iqbal, M., Han, X., Naseem, S.: Influence of cobalt doping on structural and magnetic properties of BiFeO3 nanoparticles. J. Nanoparticle Res. 17(11), 429 (2015)

Article ADS Google Scholar

31. Mukherjee, A., Basu, S., Manna, P., Yusuf, S., Pal, M.: Enhancement of multiferroic properties of nanocrystalline BiFeO 3 powder by Gd-doping. J. Alloys Compd. 598, 142–150 (2014)

Article Google Scholar

32. Ederer, C., Spaldin, N.A.: Influence of strain and oxygen vacancies on the magnetoelectric properties of multiferroic bismuth ferrite. Phys. Rev. B 71(22), 224103 (2005)

Article ADS Google Scholar

Acknowledgments

The author Mahendra V. Shisode is very much thankful to Solapur University, Solapur, for providing XRD, Department of Archaeology, Aurangabad, for the FTIR, North Maharashtra University, Jalgaon for FESEM, IIT Madras, Chennai, for the VSM, Savitribai Phule Pune University, Pune for P-E characterization facilities.

Author information

Authors and Affiliations

Department of Physics, Dr. Babasaheb Ambedkar Marathwada University, Aurangabad, MS, India
Mahendra V. Shisode, Dhananjay N. Bhoyar, Pankaj P. Khirade & K. M. Jadhav

Corresponding author

Correspondence to K. M. Jadhav.

Rights and permissions

About this article

Cite this article

Shisode, M.V., Bhoyar, D.N., Khirade, P.P. *et al.* Structural, Microstructural, Magnetic, and Ferroelectric Properties of Ba^{2+}-Doped $BiFeO_3$ Nanocrystalline Multifferroic Material. *J Supercond Nov Magn* 31, 2501–2509 (2018). https://doi.org/10.1007/s10948-017-4515-5

Received	Accepted	Published
07 November 2017	04 December 2017	12 December 2017

Issue Date
August 2018

DOI
https://doi.org/10.1007/s10948-017-4515-5

Share this article

Keywords

Bismuth ferrite Multiferroic Magnetic properties Ferroelectric Sol-gel